

# MGRegBench: A Novel Benchmark Dataset with Anatomical Landmarks for Mammography Image Registration

Svetlana Krasnova<sup>a,\*</sup>, Emiliya Starikova<sup>b</sup>, Ilia Naletov<sup>b</sup>, Andrey Krylov<sup>a</sup>, Dmitry Sorokin<sup>a,\*</sup>

<sup>a</sup>*Lomonosov Moscow State University, Moscow, Russian Federation*

<sup>b</sup>*Third Opinion Platform, Moscow, Russian Federation*

---

## Abstract

Robust mammography registration is essential for clinical applications like tracking disease progression and monitoring longitudinal changes in breast tissue. However, progress has been limited by the absence of public datasets and standardized benchmarks. Existing studies are often not directly comparable, as they use private data and inconsistent evaluation frameworks. To address this, we present MGRegBench, a public benchmark dataset for mammogram registration. It comprises over 5,000 image pairs, with 100 containing manual anatomical landmarks and segmentation masks for rigorous evaluation. This makes MGRegBench one of the largest public 2D registration datasets with manual annotations. Using this resource, we benchmarked diverse registration methods—including classical (ANTs), learning-based (VoxelMorph, TransMorph), implicit neural representation (IDIR), a classic mammography-specific approach, and a recent state-of-the-art deep learning method MammoRegNet. The implementations were adapted to this modality from the authors' implementations or re-implemented from scratch. Our contributions are: (1) the first public dataset of this scale with manual landmarks and masks for mammography registration; (2) the first like-for-like comparison of diverse methods on this modality; and (3) an extensive analysis of deep learning-based registration. We publicly release our code and data to establish a foundational resource for fair comparisons and catalyze future research. The source code and data are at <https://github.com/KourtKardash/MGRegBench>.

---

## 1. Introduction

Breast cancer remains the most commonly diagnosed cancer among women worldwide, accounting for 11.7% of all cancer cases and 6.6% of cancer deaths in 2022 [1], which tends to increase by 38% and 68%, respectively by 2050 [2]. Early detection through mammography screening has been shown to reduce breast cancer mortality by 39% [3]. However, tracking disease progression and assessing longitudinal changes in breast tissue pose significant challenges due to the high variability in mammographic images acquired at different time points. Mammographic images are highly sensitive to breast compression, patient positioning, and imaging protocols. The breast is a deformable organ, and variations in compression force can lead to substantial differences in tissue appearance between examinations.

---

\*Corresponding authors

Email addresses: [skrasnova005@gmail.com](mailto:skrasnova005@gmail.com) (Svetlana Krasnova), [dsorokin@cs.msu.ru](mailto:dsorokin@cs.msu.ru) (Dmitry Sorokin)

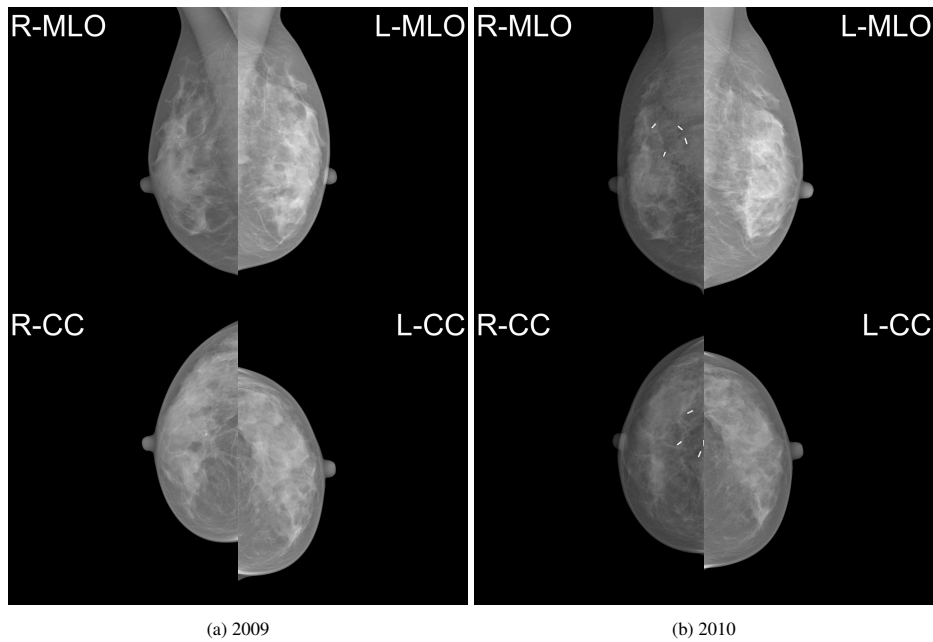


Figure 1: Example of a full-fledged paired study from INBreast dataset made in 2009 and in 2010 year correspondingly. This case is particularly illustrative due to the presence of metallic surgical clips in the right breast, indicating a prior surgical intervention.

To address these challenges, mammography image registration, the process of spatially aligning mammographic images, has emerged as a critical tool. Effective registration enables:

- Accurate tracking of lesions (like microcalcifications [4] or masses [5]) over time.
- Improved computer-aided diagnosis (CAD) by reducing false positives in longitudinal studies [6, 7, 8].

The X-ray mammography registration techniques can be broadly divided into two main categories: intensity-based [9] and feature-based [10]. Intensity-based image registration techniques directly operate on the image pixel values. In this category, the deformation needed to register one image to the other is recovered by optimizing a measure of similarity between images. Feature-based image registration techniques require defining a set of control points that must be identified and registered in each mammography. As previously mentioned, the identification of control points is a difficult task due to the compression process that produces a nonrigid structure in which few distinct anatomical landmarks exist. Despite significant progress in deep learning-based medical image registration in recent years, very few studies have applied these techniques to mammography data [11]. Nevertheless, a few recent works have explored deep learning approaches specifically for CC (Cranio-Caudal) - MLO (Medio-Lateral-Oblique) view registration, aiming to align complementary projections of the same breast [12, 13].

Despite the extensive research on mammography registration [14, 15, 16], a major limitation persists: the absence of publicly available, standardized datasets. Most existing studies rely on private, institution-specific data collected from individual hospitals or research centers [17].

While [16] introduced a CNN-based registration method for mammography, their evaluation on unannotated public datasets was limited. The authors omitted comparisons with existing registration techniques and assessed registration quality implicitly through the lens of a downstream clinical task and by pixel-wise image similarity metrics that do not account for anatomical accuracy. This creates several critical challenges for the field:

- **Lack of Reproducibility:**

Without access to the original datasets, independent reproduction and validation of published methods is impossible.

- **Incomparability of Methods:**

Different research groups use diverse evaluation metrics, datasets, and preprocessing pipelines. Some studies report landmark registration errors [18], while others focus on basic metrics such as mutual information (MI) or cross-correlation (CC) [19].

The absence of a standardized benchmark dataset hinders progress in the field. Researchers cannot objectively determine whether new methods outperform existing ones or identify which approaches work best for specific clinical scenarios (e.g., dense breasts).

To address these challenges, we introduce MGRRegBench, the first public benchmark dataset specifically designed for mammography registration. Our main contributions are:

- The dataset comprises paired mammograms from multiple patients, including a subset of 100 pairs with expert-identified anatomical landmarks and breast segmentation masks.
- We establish a standardized evaluation framework with consistent metrics and protocols to enable fair comparison of different registration methods.
- We provide comprehensive results by evaluating several widely used registration algorithms spanning a spectrum of algorithmic paradigms on our benchmark, creating the first standardized performance comparison in this domain.
- We include an extensive benchmark of modern deep learning-based registration methods, providing a crucial baseline for future research in this domain.

By providing this resource to the research community, we aim to accelerate progress in mammography registration, enable reproducible research, and facilitate the development of more robust clinical tools for longitudinal breast cancer analysis.

## **2. Review of Existing Mammography Datasets**

A number of mammography datasets have been introduced to advance research in breast cancer analysis. However, their utility for image registration task remains limited. Some datasets, such as OPTIMAM [20], LAMIS-DMDB [21], and EMBED [22], are not publicly accessible without a formal data use agreement, with EMBED explicitly prohibiting the redistribution of data. Furthermore, many publicly available datasets, including DMID [23], CMMD [24], VinDr-Mammo [25], CDD-CESM [26], CBIS-DDSM [27], and MIAS [28], lack the paired images necessary for mammography registration task. While the large-scale Mammo-Bench [29] dataset aggregates several public collections, its composite structure necessitated a detailed inspection

of each constituent dataset individually to verify the availability of paired examinations from the same patient.

In contrast to the datasets mentioned above, 3 publicly available collections include a number of patients with multiple screening exams. From these, we extracted image pairs corresponding to *the same breast* (left or right), *the same projection* (CC or MLO), and *the same patient*, ensuring consistent anatomical content and projection geometry suitable for pairwise registration. In many cases, these pairs correspond to different screening visits, making them valuable for longitudinal registration tasks.

*INbreast* [30] was introduced in 2011. It contains 115 cases, totalling 410 digital images in DICOM format. 90 cases were women with both breasts affected, each with four images, while 25 cases involved mastectomy patients; they only had two images per patient. This dataset provides detailed metadata, including patient ID, laterality, view, acquisition date, file name, breast density, BI-RADS scores, pixel-level lesion contours validated by two experts, and radiology reports.

*KAU-BCMD* [31], the King Abdulaziz University Breast Cancer Mammogram Dataset consists of 1,416 cases and 2,206 images in JPG format, collected between April 2019 and March 2020. Metadata includes study date, patient ID, patient age, laterality, view, breast density, and BI-RADS scores (determined by 3 radiologists' majority vote).

*RSNA* [32], the Radiological Society of North America Screening Mammography Breast Cancer Detection dataset features a large collection of 54,705 DICOM format images from approximately 20,000 patients. Metadata includes patient ID, image ID, laterality, view, patient age, breast density, BI-RADS score, case difficulty level, the presence of breast implants, cancer (whether or not the breast was positive for malignant cancer), biopsy (whether or not a follow-up biopsy was performed on the breast), and invasive (if the breast is positive for cancer, whether or not the cancer proved to be invasive). This screening dataset does not include segmentation or ROI annotations.

### 3. MGRRegBench Dataset

#### 3.1. Dataset Composition

Our MGRRegBench dataset is composed of mammographic images sourced from 3 publicly available datasets: *INbreast* [30], *KAU-BCMD* [31], and *RSNA* [32] (image pairs examples are shown in Figure 2).

While *INbreast* and *KAU-BCMD* include study dates, allowing us to form temporally ordered image pairs, the *RSNA* dataset does not provide this information. Consequently, in *RSNA* we can associate images only by patient ID and cannot determine the temporal order or the time interval between studies.

Each MGRRegBench image pair is accompanied by comprehensive metadata derived from the original datasets.

To facilitate rigorous benchmarking, the dataset is randomly divided into training and registration evaluation subsets. This split ensures a sufficiently large training set for deep learning methods while retaining a representative evaluation set for unbiased evaluation.

The train set contains 10,966 mammographic images, forming 5,907 pairs for registration. Designed to support the development of both classical and learning-based registration methods, including those requiring large amounts of data (e.g., *VoxelMorph*, *TransMorph*).

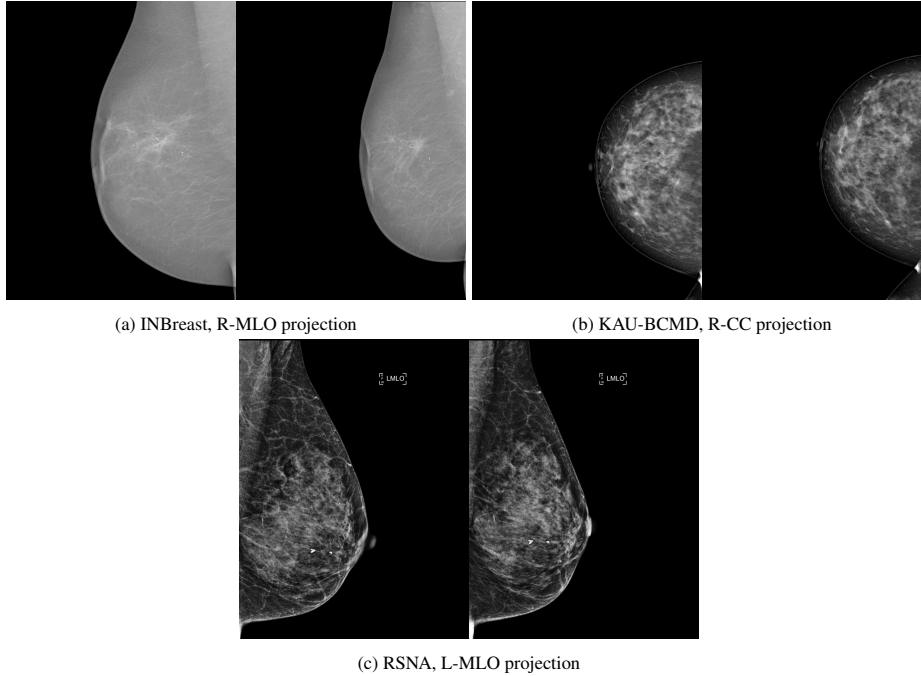


Figure 2: Example of a registration-ready image pair from each source dataset included in MGRRegBench: (left) INBreast, (center) KAU-BCMD, and (right) RSNA. Each pair shows the same breast (left or right) in the same projection (CC or MLO) acquired during separate screening exams.

The evaluation set contains 200 mammographic images, forming 100 pairs for registration. For each image from the evaluation set, we also provide a binary breast mask.

The registration evaluation set was carefully selected to closely match the training set in terms of key clinical and imaging characteristics. Specifically, the distributions of breast density and patient age (Figure 3) are approximately balanced between the two subsets. Breast density refers to the proportion of fibroglandular tissue relative to fatty tissue in the breast, a key radiological characteristic that influences both cancer risk and mammographic interpretability [33]. Examples of breasts with different densities are shown in Figure 2. The breast in the left image has a density of 1, while in the right it has a density of 4. The density classifications in our dataset use the original notation from the metadata (levels 1-4), which map to the A-D categories in [33]. Furthermore, the evaluation set contains an equal representation of all four standard mammographic views: R-MLO, R-CC, L-MLO, and L-CC, ensuring view-wise fairness in performance assessment.

A complete clinical study for a breast is defined as a paired CC and MLO view. For the INbreast and KAU-BCMD datasets, which provide examination timestamps, we reconstructed temporal pairs by identifying a patient’s complete study (L-CC, L-MLO, R-CC, R-MLO) from one time point and aligning it with a corresponding full study from a different time point. An example of a full bilateral study acquired at two different time points is shown in Figure 1.

This temporal alignment was not feasible for the RSNA dataset due to the lack of timestamp information. Consequently, for RSNA, evaluation pairs were randomly sampled from the entire

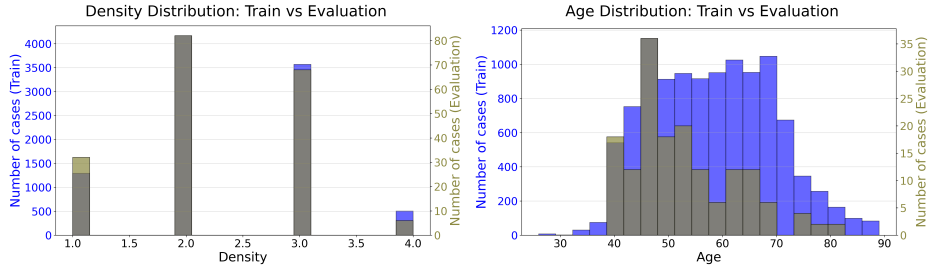


Figure 3: Overlaid histograms of patient age and breast density distributions in the training (blue, left y-axis) and evaluation (olive, right y-axis) sets. The training histograms are plotted in the background, while the evaluation histograms are overlaid in the foreground for direct visual comparison. The x-axis represents density or age category, and the two y-axes show the respective case counts.

pool of available images.

The final evaluation subset was compiled as follows:

- INbreast: 6 patients (20 image pairs). This includes 4 patients with complete bilateral studies and 2 post-mastectomy patients contributing data from a single breast across two time points.
- KAU-BCMD: 10 patients (40 image pairs), each providing a complete bilateral study across two time points.
- RSNA: 40 randomly assembled image pairs ensuring view-wise balance.

The annotation of anatomical landmarks in mammography is inherently challenging due to the overlapping nature of breast tissue, which obscures clear and consistent anatomical landmarks — a difficulty that is also recognized in other areas of deformable 2D medical imaging domains [34]. Despite this, our dataset includes 100 expert-annotated image pairs, each labeled with approximately 10 clinically meaningful landmarks. This places MGRRegBench among the most substantial publicly available 2D registration benchmarks with manual landmark annotations. For context, the FIRE fundus registration dataset includes 134 image pairs with 10 landmarks each [35]; the fetal brain ultrasound benchmark provides 25 landmarks across all 104 images [36]; and the thorax X-ray/CT registration dataset uses only 8 landmarks per image due to anatomical ambiguity [34].

Furthermore, our evaluation set was constructed via stratified sampling to ensure proportional representation of various clinical challenges, such as varying breast density, patient age and postoperative cases. This strategy guarantees that performance metrics are not biased toward easy cases but reflect algorithm robustness across the full spectrum of real-world scenarios, making the benchmark clinically relevant.

### 3.2. Anatomical Landmarks Annotation

Anatomical landmarks are provided exclusively for the evaluation subset of MGRRegBench, enabling quantitative evaluation of registration accuracy. These landmarks include calcifications, duct or blood vessel bends, intersections, forks, visible masses and dark or bright blobs (Figure 4).

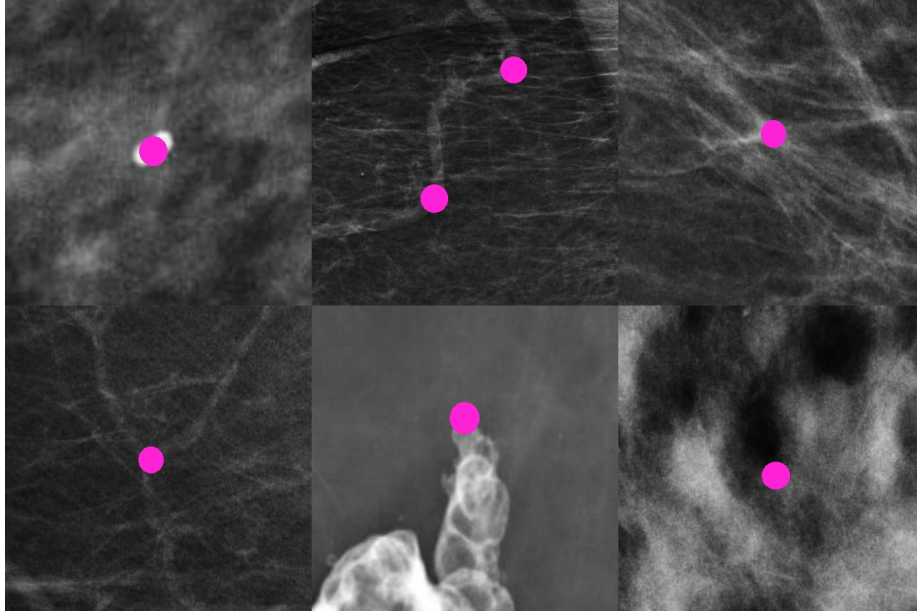


Figure 4: Examples of anatomical landmarks used for registration evaluation in MGRegBench. Each panel illustrates a distinct landmark type manually annotated by expert radiologists: microcalcifications, bends in ducts or blood vessels, vessel or duct intersections, forks, visible masses, and dark/bright blob contours.

Annotations were generated using CVAT tool [37] in two phases by two professional radiologists. Annotation protocols for both phases, including an example of what constitutes corresponding landmark locations, are available online.

During the first phase, the first annotator was asked to place 12-15 corresponding landmarks in an mammography pair that was displayed side-by-side in CVAT. This initial annotation of 100 image pairs required 31.6 hours of radiologist time. For the second phase, landmarks in the left image were fixed in place and displayed, whereas landmarks in the right one were deleted. The second annotator was then tasked with determining landmarks on the right side to the locations that they considered to match the displayed landmarks on the left side. This crucial validation phase required even more meticulous effort, taking approximately 63 hours to complete for the same set of 100 pairs. An example of landmark annotation is shown in the Figure 5.

We computed the localization error as the Euclidean distance between corresponding landmark locations annotated independently by two expert radiologists. To account for varying image resolutions, the error was normalized by corresponding image diagonal. Outliers were identified using the interquartile range ( $IQR$ ) method: a normalized error was considered an outlier if it exceeded the threshold  $T$  defined as

$$T = Q_3 + 1.5IQR, \quad (1)$$

where  $Q_1$  and  $Q_3$  denote the 25th and 75th percentiles, respectively, of the normalized localization error distribution computed over all annotated landmark pairs, and  $IQR = Q_3 - Q_1$ .

After applying the outlier filtering criterion, 180 out of the initial 1,196 annotated landmark pairs were excluded, corresponding to approximately 15% of the total. The average localization error between corresponding landmark locations after filtering is 0.34%.

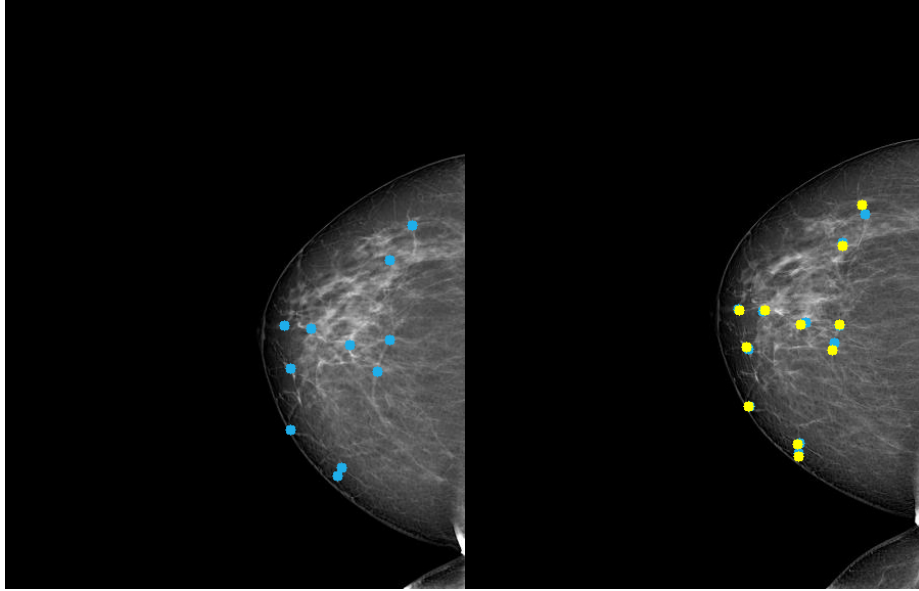


Figure 5: Example of landmark annotation performed by two radiologists. Blue markers indicate landmarks placed during the initial annotation phase; yellow markers show the refined annotations from the second (validation) phase.

### 3.3. Breast Segmentation

Each image in the evaluation subset was accompanied by a binary segmentation mask. These masks were produced through a three-step process: initial manual labeling, subsequent semi-automatic post-processing, and final manual validation and correction.

### 3.4. Dataset Structure

The MGRRegBench dataset is organized into *train* and *evaluation* directories for method development and performance assessment, respectively.

Data in both directories are grouped by source datasets (*INBreast*, *KAU-BCMD*) within patient-specific folders named with anonymized IDs. Each patient folder contains 2 (or more in some cases) images: PNG (and original DICOM) for *INBreast* and JPG for *KAU-BCMD*.

Due to licensing, the RSNA dataset is not redistributed. Instead, we provide a script that, when run on a local copy of the official RSNA dataset, extracts the relevant image pairs and integrates them into the MGRRegBench structure in PNG format (preserving original DICOMs), ensuring reproducibility while complying with data agreements.

Ground-truth breast segmentation masks are in the *evaluation-masks* directory, mirroring the image structure. Masks for all 3 source datasets are stored in PNG format.

Expert anatomical landmark annotations for the evaluation set are in 3 separate XML files: (1) landmarks by the first radiologist on the first image of each pair, (2) corresponding landmarks by the same radiologist on the second image, and (3) independent annotations by a second radiologist on the second image for inter-observer validation.

## 4. Benchmark Study

### 4.1. Registration Methods

For mammography image registration, we employed 7 representative methods spanning a spectrum of algorithmic paradigms:

- ANTs (SyN) [38, 39] as a widely adopted classical method being standard in medical image registration;
- A curvilinear coordinate-based method [18] explicitly designed for breast anatomy by aligning images along tissue-structure-aware coordinate systems;
- IDIR [40], a coordinate-based method using implicit neural representations (INRs), which models deformation as a continuous function for inherent smoothness and generalization.
- VoxelMorph [41] and TransMorph [42] as most common well-founded deep learning-based approaches that learn deformable registration from data, with TransMorph leveraging transformer architectures to capture long-range spatial dependencies;
- MammoRegNet [16] as a recent state-of-the-art deep learning method designed for 2D mammography data.

All deep learning methods were preceded by initial affine alignment performed with ANTs [38] to ensure robust convergence. MammoRegNet incorporates an affine alignment stage within its architecture. To assess the impact of external initialization, we report two variants: (1) MammoRegNet applied without external affine pre-alignment and (2) MammoRegNet preceded by an affine transform computed with ANTs [38]. We report the performance of this affine baseline alongside the full results to explicitly demonstrate the incremental improvement achieved by the more complex, non-rigid registration algorithms.

ANTs (SyN) served as a classical, intensity-based baseline. We used the default parameters of the Symmetric Normalization algorithm without any modality-specific tuning.

The curvilinear coordinate-based method incorporates breast-specific anatomical priors to constrain the deformation field, ensuring physically plausible alignments. It represents the current state-of-the-art among non-learning methods explicitly designed for mammographic registration. As the original work does not provide an official implementation, we release our re-implementation to ensure reproducibility and facilitate future research.

We adapted IDIR for 2D data and trained it across 5 random seeds to mitigate its known sensitivity to initialization. Since averaging metrics across all seeds was skewed by outliers, we used a robust aggregation strategy: for each image pair, we picked the result from its best-performing seed to compute final metrics. Training used a batch size of 2,500 over 2,500 epochs with a  $10^{-4}$  learning rate, ReLU activation, and 0.01 Jacobian deformation regularization weight.

VoxelMorph and TransMorph were adapted to 2D and trained on the MGRRegBench train set for 1,500 epochs (100 iterations/epoch) with a batch size of 1. Using an MSE loss, all hyperparameters were adopted from the original implementations except the deformation regularization weight, which was experimentally tuned to 1 to ensure smooth, fold-minimized deformations.

Finally, MammoRegNet was employed without any modifications and trained for 1,500 epochs (100 iterations/epoch) with a batch size of 1, using the hyperparameters specified by the authors.

## 4.2. Metrics

To provide a comprehensive and clinically meaningful evaluation of registration performance, we employ a diverse set of metrics spanning anatomical accuracy, intensity-based similarity, segmentation-based overlap, deformation regularity, and computational efficiency.

**Anatomical accuracy.** Anatomical accuracy is assessed using the relative Target Registration Error (rTRE), computed on expert-annotated corresponding landmarks. The rTRE is defined as the Euclidean distance between corresponding landmarks in the transformed moving image ( $I_M$ ) and the fixed image ( $I_F$ ), normalized by the image diagonal length and expressed as a percentage:

$$\text{rTRE}_l = \frac{\|\mathbf{x}_l^M - \mathbf{x}_l^F\|_2}{d} \cdot 100, \quad (2)$$

where  $\mathbf{x}_l^M$  and  $\mathbf{x}_l^F$  are the landmarks,  $d$  is the image diagonal length.

To obtain a robust estimate of registration error with both intra- and inter-observer uncertainty in landmark placement, we employed the following evaluation protocol:

(1) compute the mean Euclidean distance between the first annotator’s landmarks on the moving image (after warping) and their corresponding landmarks on the fixed image (also by the first annotator); (2) compute the mean distance between the same warped moving landmarks and the second annotator’s landmarks on the fixed image; (3) average these two distances per image pair; (4) finally, average the result across all pairs in the evaluation set.

**Intensity-based similarity metrics.** Intensity-based similarity is evaluated using 4 complementary metrics:

- Mean Squared Error (MSE) measures pixel-wise intensity differences;
- Structural Similarity Index (SSIM) quantifies perceptual similarity;
- Mutual Information (MI) evaluates the statistical dependence between image intensities;
- Cross-Correlation (CC) assesses the linear correlation of intensity values;

**Deformation regularity metric.** Deformation regularity is critical for clinical plausibility. The foldings of the deformation field were measured using the percentage of negative Jacobian determinants (NJD).

**Segmentation-based metric.** Binary breast tissue masks are available for every image in the evaluation set. A moving mask is warped by the deformation field, enabling per-pair computation of segmentation-based metrics after registration. Specifically, we compute the Dice Similarity Coefficient (DSC) to quantify overlap.

**Computational efficiency measurements.** To assess practical deployment potential, we measure computational efficiency:

- GPU memory (VRAM) usage during inference and training (for trainable methods).;
- Runtime per image pair for inference and total training time (for trainable methods).

Experiments were run on an Intel Xeon Gold 6226R CPU / NVIDIA A6000 GPU server.

Together, these metrics provide a holistic view of registration quality – balancing anatomical fidelity, image similarity, and real-world usability.

Table 1: Quantitative evaluation of mammography registration methods on the MGRRegBench dataset. The best results are in **bold**. †Training / Inference time or memory.

Metric	Unreg.	Affine	SyN [39]	Curv. coord. [18]	IDIR [40]	VM [41]	TM [42]	MRN [16]	Affine + MRN [16]
rTRE (%) ↓	4.5352	2.1392	2.1021	4.18	2.461	2.1372	2.1377	2.5082	<b>2.0276</b>
MSE ↓	782.493	451.8501	379.5068	594.249	418.697	326.1821	258.5715	141.7426	<b>130.3179</b>
SSIM ↑	0.7587	0.8024	0.8212	0.7994	0.8107	0.8065	0.81	0.8392	<b>0.8449</b>
MI ↑	1.1832	1.2441	1.267	1.2336	1.26	1.2573	1.2652	1.2956	<b>1.3027</b>
CC ↑	0.8261	0.8912	0.9112	0.8592	0.9077	0.9187	0.933	0.9676	<b>0.9705</b>
NJD (%) ↓	–	–	1.5e-05	0.9497	<b>0</b>	9.5e-05	1.43e-04	0.0972	0.1379
DSC ↑	0.9206	0.9711	0.9777	0.9665	0.95	0.9787	0.9859	0.991	<b>0.9921</b>
VRAM (Gb) ↓	–	–	–	–	8.4	1.025 / 0.43†	4.834 / 1.815†	1.114 / <b>0.36†</b>	1.114 / <b>0.36†</b>
Runtime ↓	–	2.1979 s	8.3589 s	183.9785 s	29.96 s	12.5 h / 0.5598 s†	32.083 h / 1.3908 s†	9.08 h / <b>0.2515 s†</b>	28.3 h / 1.2293 s†

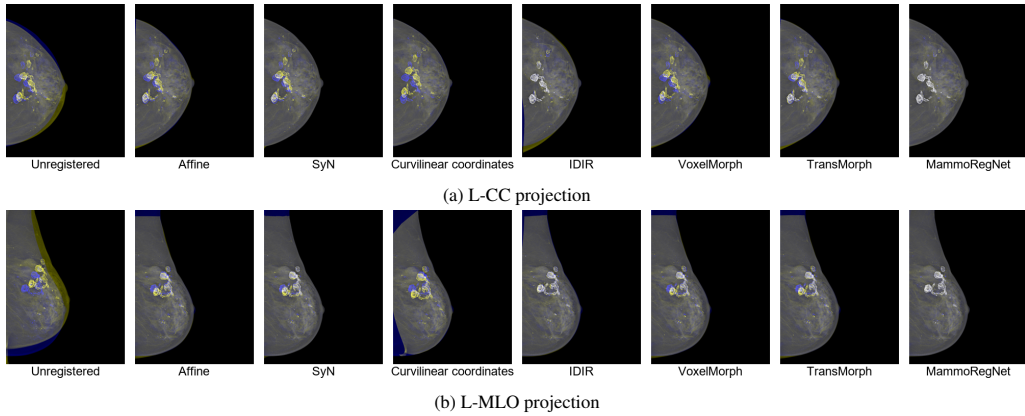


Figure 6: Registration results for an example pair in the L-CC and L-MLO projections. The overlays show the fixed image (in blue) and the moved image (in yellow) after registration using different methods: unregistered, Affine, SyN, Curvilinear Coordinates, IDIR, VoxelMorph, TransMorph, and MammoRegNet. Successful alignment is indicated by the overlap of corresponding anatomical structures in white.

### 4.3. Results

The quantitative evaluation of all registration methods on the MGRRegBench benchmark is presented in Table 1, with visual examples of registration outcomes shown in Figure 6 for CC and MLO projections. Visual inspection of the registration results reveals notable differences across methods. While IDIR does not achieve perfect alignment of the breast boundary, it demonstrates accurate correspondence of the internal masses, suggesting effective modeling of local deformations. In contrast, the curvilinear coordinates–based method yields the poorest visual alignment among all evaluated approaches. Moreover, due to its geometric formulation, this method truncates a portion of the breast tissue (it’s particularly evident in the MLO projection) which may lead to loss of diagnostically relevant information. TransMorph exhibits slightly superior visual alignment compared to VoxelMorph (especially in the CC view) consistent with its more expressive transformer-based architecture. Nevertheless, ANTs, VoxelMorph, and TransMorph produce comparable overall performance: in all three cases, the masses are only partially overlapped, indicating residual misalignment. MammoRegNet with affine preprocessing achieves visually superior alignment compared to all other methods, with perfect overlap of both breast

boundaries and internal anatomical structures.

For anatomical accuracy the combined Affine + MRN method achieves the best rTRE result (2.0276%), followed by the classical ANTs (SyN) method (2.1021%). Among deep learning approaches, VoxelMorph (2.1372%) and TransMorph (2.1377%) demonstrate competitive performance. The standalone MammoRegNet (2.5082%) and IDIR (2.461%) yield slightly higher errors. In contrast, the curvilinear coordinate method exhibits the worst landmark alignment (4.18%), indicating that its geometric parametrization is ill-suited for the complex deformations observed in mammography.

For intensity-based similarity metrics and segmentation-based overlap, the Affine + MRN pipeline consistently achieves the best scores, with the lowest MSE (130.3179) and the highest SSIM (0.8449), MI (1.3027), CC (0.9705), and DSC (0.9921). Standalone MammoRegNet ranks a close second across these metrics. TransMorph, VoxelMorph follow, showing robust performance, particularly in MSE and CC. The curvilinear coordinates-based method shows moderate performance, as it matches the overall geometry rather than pixel-level intensities.

To summarize, the standalone MammoRegNet achieves state-of-the-art performance in intensity-based similarity and segmentation overlap but exhibits a relatively high rTRE (2.5082%). This degradation in landmark accuracy is driven by outliers where large initial misalignments lead to implausible deformations, highlighting the model’s sensitivity to global pose variations. In contrast, the Affine + MRN pipeline mitigates this issue by first resolving coarse misalignment through an affine transform, which significantly improves robustness. This hybrid approach not only reduces rTRE to the lowest among all methods (2.0276%) but also further enhances intensity-based metrics.

The percentage of pixels with a negative Jacobian determinant (NJD) reflects the degree of folding in the deformation field. IDIR achieves a perfect NJD of 0% while ANTs (SyN), VoxelMorph and TransMorph show a near-zero value (1.5e-05%, 9.5e-05% and 1.43e-04% respectively), indicating high smoothness. Among deep learning methods MammoRegNet (0.0972%) and Affine + MRN (0.1379%) exhibit substantially higher NJD, indicating noticeable folds in their deformation fields.

Finally, computational efficiency varies significantly. MammoRegNet offers the fastest inference (0.2515 s/pair) and the lowest VRAM usage during inference (0.36 GB) among the deep learning methods. The combined Affine + MRN pipeline has a longer inference time (1.2293 s) due to the sequential processing but retains the same memory footprint. VoxelMorph and TransMorph also provide fast inference but with higher memory consumption. In contrast, IDIR is slower (30 s/pair) and more memory-intensive (8.4 GB). ANTs runs in 8.36 s/pair on CPU, while the curvilinear method is the slowest.

#### 4.4. Discussion

The trends observed in our benchmark largely mirror those reported in the broader medical image registration field. As discussed in [43], classical optimization-based methods such as ANTs (SyN) [39] often remain competitive or superior to deep learning (DL) approaches when evaluated on anatomical accuracy. In our results, ANTs (SyN) [39] achieves the second-best rTRE. However, the best anatomical accuracy is attained by a hybrid approach Affine + MRN [16] that combines a classical affine step with a deep learning model. This suggests that integrating classical and learning-based paradigms can leverage their respective strengths.

Our observations also align with findings from [44]. While that INR-based approach demonstrated stable and smooth deformations across modalities, its evaluation on the DIRLab dataset

[45] showed that classical pTV algorithm [46] still achieved superior accuracy compared to all deep learning methods, including implicit neural representations. This outcome is consistent with our finding that ANTs (SyN) remains highly competitive on the landmark-based rTRE metric.

## 5. Clinical significance

Accurate registration of longitudinal mammograms is a critical prerequisite for a range of clinical applications, including change detection, lesion tracking, and computer-aided diagnosis [47, 48, 49, 50]. Subtle temporal changes in breast tissue – such as the emergence or growth of masses, or microcalcification clusters – are often the earliest signs of malignancy [51]. Reliable alignment of prior and current exams enables radiologists and AI systems to focus on true biological changes rather than misregistration artifacts caused by differences in patient positioning, compression, or anatomy.

The MRegBench benchmark, with its expert-annotated anatomical landmarks and diverse clinical scenarios, including post-surgical cases with metallic clips and varying breast densities, provides a realistic testbed for evaluating registration algorithms under conditions that reflect routine screening practice. By establishing standardized protocols and performance metrics, our work supports the development of robust registration tools that can ultimately enhance diagnostic accuracy, reduce false positives in longitudinal screening, and facilitate quantitative monitoring of disease progression or treatment response.

## 6. Conclusion

We have introduced MRegBench, the first public benchmark dataset for mammography registration, comprising 100 expert-annotated image pairs and a large training set derived from INbreast, KAU-BCMD, and RSNA. By providing standardized data, metadata, and evaluation protocols our benchmark addresses critical gaps in reproducibility and method comparison that have long hindered progress in the field.

Our evaluation of 7 representative registration methods establishes Affine+MRN as the current state-of-the-art, excelling in both intensity-based metrics and anatomical accuracy, albeit producing less smooth deformations. While standalone MRN performs well on intensity measures, it yields the second worst rTRE. ANTs (SyN) ranks second in rTRE but generates smooth deformations. To foster reproducible research and accelerate the development of registration methods, including methods for analyzing longitudinal disease progression, we publicly release our dataset and baseline implementations (the link is provided in the abstract). We believe that the presented benchmark and dataset will serve as a vital resource for developing novel, specialized methods for mammography image registration and longitudinal disease progression analysis.

## References

- [1] I. A. for Research on Cancer, et al., Breast Cancer Cases and Deaths Are Projected to Rise Globally (2025).
- [2] J. Kim, A. Harper, V. McCormack, H. Sung, N. Houssami, E. Morgan, M. Mutebi, G. Garvey, I. Soerjomataram, M. M. Fidler-Benaoudia, Global Patterns and Trends in Breast Cancer Incidence and Mortality Across 185 Countries, *Nature Medicine* (2025) 1–9.

- [3] N. J. Massat, A. Dibden, D. Parmar, J. Cuzick, P. D. Sasieni, S. W. Duffy, Impact of screening on breast cancer mortality: the uk program 20 years on, *Cancer Epidemiology, Biomarkers & Prevention* 25 (3) (2016) 455–462.
- [4] R. Zamir, S. Bagon, D. Samocha, Y. Yagil, R. Basri, M. Sklair-Levy, M. Galun, Segmenting Microcalcifications in Mammograms and Its Applications, in: *Medical Imaging 2021: Image Processing*, Vol. 11596, SPIE, 2021, pp. 788–795.
- [5] A. Varlamova, V. Belotsky, G. Novikov, A. Konushin, E. Sidorov, Features Fusion For Dual-View Mammography Mass Detection, in: *2024 IEEE International Symposium on Biomedical Imaging (ISBI)*, IEEE, 2024, pp. 1–5.
- [6] Y. Shen, F. E. Shamout, J. R. Oliver, J. Witowski, K. Kannan, J. Park, N. Wu, C. Huddleston, S. Wolfson, A. Millet, et al., Artificial Intelligence System Reduces False-positive Findings in the Interpretation of Breast Ultrasound Exams, *Nature Communications* 12 (1) (2021) 5645.
- [7] R. C. Mayo, D. Kent, L. C. Sen, M. Kapoor, J. W. Leung, A. T. Watanabe, Reduction of False-positive Markings on Mammograms: a Retrospective Comparison Study Using an Artificial Intelligence-based CAD, *Journal of Digital Imaging* 32 (4) (2019) 618–624.
- [8] K. Loizidou, G. Skouroumouni, C. Nikolaou, C. Pitris, A Review of Computer-aided Breast Cancer Diagnosis Using Sequential Mammograms, *Tomography* 8 (6) (2022) 2874–2892.
- [9] Y. Díez, A. Oliver, X. Llado, J. Freixenet, J. Marti, J. C. Vilanova, R. Marti, Revisiting intensity-based image registration applied to mammography, *IEEE Transactions on Information Technology in Biomedicine* 15 (5) (2011) 716–725.
- [10] S. S. Brandt, G. Karemore, N. Karssemeijer, M. Nielsen, An anatomically oriented breast coordinate system for mammogram analysis, *IEEE Transactions on Medical Imaging* 30 (10) (2011) 1841–1851.
- [11] J. Li, X. Wang, C. Qian, Mammography Registration for Unsupervised Learning Based on CC and MLO views, in: *Proceedings of the 2020 3rd International Conference on Artificial Intelligence and Pattern Recognition*, 2020, pp. 157–162.
- [12] W. C. Walton, S.-J. Kim, S. C. Harvey, L. A. Mullen, D. W. Porter, Towards CNN-based Registration of Craniocaudal and Mediolateral Oblique 2-D X-ray Mammographic Images, in: *2019 41st Annual International Conference of the IEEE Engineering in Medicine and Biology Society (EMBC)*, IEEE, 2019, pp. 2758–2764.
- [13] W. C. Walton, S.-J. Kim, L. A. Mullen, Automated Registration for Dual-view X-ray Mammography Using Convolutional Neural Networks, *IEEE Transactions on Biomedical Engineering* 69 (11) (2022) 3538–3550.
- [14] S. van Engeland, P. Snoeren, J. Hendriks, N. Karssemeijer, A comparison of methods for mammogram registration, *IEEE Transactions on Medical Imaging* 22 (11) (2003) 1436–1444.
- [15] J. H. Hipwell, V. Vavourakis, L. Han, T. Mertzaniidou, B. Eiben, D. J. Hawkes, A review of biomechanically informed breast image registration, *Physics in Medicine & Biology* 61 (2) (2016) R1.

- [16] S. Thrun, S. Hansen, Z. Sun, N. Blum, S. A. Salahuddin, K. Wickstrøm, E. Wetzer, R. Jenssen, M. Stille, M. Kampffmeyer, Reconsidering Explicit Longitudinal Mammography Alignment for Enhanced Breast Cancer Risk Prediction, in: International Conference on Medical Image Computing and Computer-Assisted Intervention, Springer, 2025, pp. 495–505.
- [17] K. Loizidou, G. Skouroumouni, C. Nikolaou, C. Pitris, Automatic breast mass segmentation and classification using subtraction of temporally sequential digital mammograms, *IEEE Journal of Translational Engineering in Health and Medicine* 10 (2022) 1–11.
- [18] M. Abdel-Nasser, A. Moreno, D. Puig, Temporal Mammogram Image Registration Using Optimized Curvilinear Coordinates, *Computer Methods and Programs in Biomedicine* 127 (2016) 1–14.
- [19] J. M. Celaya-Padilla, J. Rodriguez-Rojas, V. Trevino, J. G. Tamez-Pena, Local image registration a comparison for bilateral registration mammography, in: IX International Seminar on Medical Information Processing and Analysis, Vol. 8922, SPIE, 2013, pp. 299–307.
- [20] M. D. Halling-Brown, L. M. Warren, D. Ward, E. Lewis, A. Mackenzie, M. G. Wallis, L. S. Wilkinson, R. M. Given-Wilson, R. McAvinchey, K. C. Young, OPTIMAM Mammography Image Database: a Large-scale Resource of Mammography Images and Clinical Data, *Radiology: Artificial Intelligence* 3 (1) (2020) e200103.
- [21] O. Imane, A. Mohamed, R. F. Lazhar, S. Hama, B. Elhadj, A. Conci, LAMIS-DMDB: a New Full Field Digital Mammography Database for Breast Cancer AI-CAD Researches, *Biomedical Signal Processing and Control* 90 (2024) 105823.
- [22] J. J. Jeong, B. L. Vey, A. Bhimireddy, T. Kim, T. Santos, R. Correa, R. Dutt, M. Mosunjac, G. Oprea-Ilieș, G. Smith, et al., The EMory BrEast Imaging Dataset (EMBED): A Racially Diverse, Granular Dataset of 3.4 Million Screening and Diagnostic Mammographic Images, *Radiology: Artificial Intelligence* 5 (1) (2023) e220047.
- [23] P. Oza, U. Oza, R. Oza, P. Sharma, S. Patel, P. Kumar, B. Gohel, Digital Mammography Dataset for Breast Cancer Diagnosis Research (DMID) with Breast Mass Segmentation Analysis, *Biomedical Engineering Letters* 14 (2) (2024) 317–330.
- [24] H. Cai, J. Wang, T. Dan, J. Li, Z. Fan, W. Yi, C. Cui, X. Jiang, L. Li, An Online Mammography Database with Biopsy Confirmed Types, *Scientific Data* 10 (1) (2023) 123.
- [25] H. T. Nguyen, H. Q. Nguyen, H. H. Pham, K. Lam, L. T. Le, M. Dao, V. Vu, VinDr-Mammo: a Large-scale Benchmark Dataset for Computer-aided Diagnosis in Full-field Digital Mammography, *Scientific Data* 10 (1) (2023) 277.
- [26] R. Khaled, M. Helal, O. Alfarghaly, O. Mokhtar, A. Elkorany, H. El Kassas, A. Fahmy, Categorized Contrast Enhanced Mammography Dataset for Diagnostic and Artificial Intelligence Research, *Scientific data* 9 (1) (2022) 122.
- [27] R. S. Lee, F. Gimenez, A. Hoogi, K. K. Miyake, M. Gorovoy, D. L. Rubin, A Curated Mammography Data Set for Use in Computer-aided Detection and Diagnosis Research, *Scientific data* 4 (1) (2017) 1–9.

- [28] J. Suckling, J. Parker, D. Dance, S. Astley, I. Hutt, C. Boggis, I. Ricketts, E. Stamatakis, N. Cerneaz, S. Kok, P. Taylor, D. Betal, J. Savage, Mammographic Image Analysis Society (MIAS) Database v1.21 (2015). doi:10.17863/CAM.105113.  
URL <https://www.repository.cam.ac.uk/handle/1810/250394>
- [29] G. Bhole, S. Suba, N. Parekh, Mammo-Bench: A Large-scale Benchmark Dataset of Mammography Images, medRxiv (2025). arXiv:<https://www.medrxiv.org/content/early/2025/10/14/2025.01.31.25321510.full.pdf>, doi:10.1101/2025.01.31.25321510.  
URL <https://www.medrxiv.org/content/early/2025/10/14/2025.01.31.25321510>
- [30] I. C. Moreira, I. Amaral, I. Domingues, A. Cardoso, M. J. Cardoso, J. S. Cardoso, Inbreast: toward a full-field digital mammographic database, *Academic radiology* 19 (2) (2012) 236–248.
- [31] A. S. Alsolami, W. Shalash, W. Alsaggaf, S. Ashoor, H. Refaat, M. Elmogy, King Abdulaziz University Breast Cancer Mammogram Dataset (Kau-bcmd), *Data* 6 (11) (2021) 111.
- [32] C. Carr, P. Felipe Kitamura, MD, G. Partridge, Inversion, J. Kalpathy-Cramer, J. Mongan, K. Andriole, Lavender, M. Vazirabad, M. Riopel, R. Ball, S. Dane, Y. Chen, RSNA Screening Mammography Breast Cancer Detection, <https://kaggle.com/competitions/rsna-breast-cancer-detection>, Kaggle (2022).
- [33] D. A. Spak, J. Plaxco, L. Santiago, M. Dryden, B. Dogan, BI-RADS® fifth edition: A summary of changes, *Diagnostic and Interventional Imaging* 98 (3) (2017) 179–190.
- [34] W. Xia, Q. Jin, C. Ni, Y. Wang, X. Gao, Thorax X-ray and CT Interventional Dataset for Nonrigid 2D/3D Image Registration Evaluation, *Medical Physics* 45 (11) (2018) 5343–5351.
- [35] C. Hernandez-Matas, X. Zabulis, A. Triantafyllou, P. Anyfanti, S. Douma, A. A. Argyros, FIRE: Fundus Image Registration Dataset, *Artificial Intelligence in Vision and Ophthalmology* 1 (4) (2017) 16–28.
- [36] M. Cabezas, Y. Diez, C. Martinez-Diago, A. Maroto, A Benchmark for 2D Foetal Brain Ultrasound Analysis [dataset] (2024).
- [37] Intel Corporation, Computer Vision Annotation Tool (CVAT, version 2.14.0 (2024)).  
URL <https://github.com/openvinotoolkit/cvat>
- [38] B. B. Avants, N. Tustison, G. Song, et al., Advanced normalization tools (ants), *Insight j* 2 (365) (2009) 1–35.
- [39] B. Avants, C. Epstein, M. Grossman, J. Gee, Symmetric Diffeomorphic Image Registration with Cross-correlation: Evaluating Automated Labeling of Elderly and Neurodegenerative Brain, *Medical Image Analysis* 12 (1) (2008) 26–41.
- [40] J. M. Wolterink, J. C. Zwienenberg, C. Brune, Implicit Neural Representations for Deformable Image Registration, in: *Proceedings of the 5th International Conference on Medical Imaging with Deep Learning (MIDL)*, PMLR, 2022, pp. 1349–1359.

- [41] G. Balakrishnan, A. Zhao, M. Sabuncu, J. Guttag, A. V. Dalca, VoxelMorph: A Learning Framework for Deformable Medical Image Registration, *IEEE Transactions on Medical Imaging* 38 (2019) 1788–1800.
- [42] J. Chen, E. C. Frey, Y. He, W. P. Segars, Y. Li, Y. Du, TransMorph: Transformer for Unsupervised Medical Image Registration, *Medical Image Analysis* 78 (2022) 102615. doi:10.1016/j.media.2022.102615. URL <https://arxiv.org/abs/2111.10480>
- [43] R. Jena, D. Sethi, P. Chaudhari, J. Gee, Deep learning in medical image registration: Magic or mirage?, *Advances in Neural Information Processing Systems* 37 (2024) 108331–108353.
- [44] L. D. Van Harten, J. Stoker, I. Išgum, Robust deformable image registration using cycle-consistent implicit representations, *IEEE Transactions on Medical Imaging* 43 (2) (2023) 784–793.
- [45] R. Castillo, E. Castillo, R. Guerra, V. E. Johnson, T. McPhail, A. K. Garg, T. Guerrero, A framework for evaluation of deformable image registration spatial accuracy using large landmark point sets, *Physics in Medicine & Biology* 54 (7) (2009) 1849.
- [46] V. Vishnevskiy, T. Gass, G. Szekely, C. Tanner, O. Goksel, Isotropic total variation regularization of displacements in parametric image registration, *IEEE transactions on medical imaging* 36 (2) (2016) 385–395.
- [47] H. Lee, J. Kim, E. Park, M. Kim, T. Kim, T. Kooi, Enhancing breast cancer risk prediction by incorporating prior images, in: *International Conference on Medical Image Computing and Computer-Assisted Intervention*, Springer, 2023, pp. 389–398.
- [48] S. Dadsetan, D. Arefan, W. A. Berg, M. L. Zuley, J. H. Sumkin, S. Wu, Deep learning of longitudinal mammogram examinations for breast cancer risk prediction, *Pattern recognition* 132 (2022) 108919.
- [49] B. K. Karaman, K. Dodelzon, G. B. Akar, M. R. Sabuncu, Longitudinal mammogram risk prediction, in: *International Conference on Medical Image Computing and Computer-Assisted Intervention*, Springer, 2024, pp. 437–446.
- [50] X. Wang, T. Tan, Y. Gao, E. Marcus, L. Han, A. Portaluri, T. Zhang, C. Lu, X. Liang, R. Beets-Tan, et al., Ordinal Learning: Longitudinal Attention Alignment Model for Predicting Time to Future Breast Cancer Events from Mammograms, in: *International Conference on Medical Image Computing and Computer-Assisted Intervention*, Springer, 2024, pp. 155–165.
- [51] S. Azam, M. Eriksson, A. Sjölander, M. Gabrielson, R. Hellgren, K. Czene, P. Hall, Mammographic microcalcifications and risk of breast cancer, *British journal of cancer* 125 (5) (2021) 759–765.